Acoustic Transmission Factor through the Rat Skull as a Function of Body Mass, Frequency and Position

Matthieu Gerstenmayer, Benjamin Fellah, Remi Magnin, Erwan Selingue, Benoit Larrat

Our reference: UMB 11221

AUTHOR QUERY FORM

ELSEVIER	**Journal: UMB** **Article Number: 11221**	**Please e-mail your responses and any corrections to:** **E-mail: correctionsaptara@elsevier.com**

Dear Author,

Please check your proof carefully and mark all corrections at the appropriate place in the proof (e.g., by using on-screen annotation in the PDF file) or compile them in a separate list. Note: if you opt to annotate the file with software other than Adobe Reader then please also highlight the appropriate place in the PDF file. To ensure fast publication of your paper please return your corrections within 48 hours.

Your article is registered as a regular item and is being processed for inclusion in a regular issue of the journal. If this is NOT correct and your article belongs to a Special Issue/Collection please contact C.Newman@elsevier.com immediately prior to returning your corrections.

For correction or revision of any artwork, please consult http://www.elsevier.com/artworkinstructions

Any queries or remarks that have arisen during the processing of your manuscript are listed below and highlighted by flags in the proof. Click on the 'Q' link to go to the location in the proof.

Location in article	Query / Remark: click on the Q link to go Please insert your reply or correction at the corresponding line in the proof
Q1	AU: The author names have been tagged as given names and surnames (surnames are highlighted in teal color). Please confirm if they have been identified correctly.
Q2	This section comprises references that occur in the reference list but not in the body of the text. Please position each reference in the text or, alternatively, delete it.
Q3	AU: Please cite Keenan et al. 1997 or delete reference from list.
	Please check this box or indicate your approval if you have no corrections to make to the PDF file. ☐

Thank you for your assistance.

Ultrasound in Med. & Biol., Vol. ■, No. ■, pp. ■■■–■■■, 2018

0301-5629/$ - see front matter

https://doi.org/10.1016/j.ultrasmedbio.2018.06.005

● *Original Contribution*

ACOUSTIC TRANSMISSION FACTOR THROUGH THE RAT SKULL AS A FUNCTION OF BODY MASS, FREQUENCY AND POSITION

Q1 MATTHIEU GERSTENMAYER, BENJAMIN FELLAH, RÉMI MAGNIN, ERWAN SELINGUE, and BENOIT LARRAT

NeuroSpin, Institut pour les sciences du vivant Frédéric Joliot, Direction de la Recherche Fondamentale, Commissariat à l'Energie Atomique, Université Paris Saclay, Gif sur Yvette, France

(*Received* 11 *December* 2017; *revised* 7 *June* 2018; *in final from* 8 *June* 2018)

Abstract—In many transcranial ultrasound studies on rats, the transmission factor is assumed to be independent of animal weight and losses because non-normal incidence angles of the beam are not accounted for. In this study, we measured acoustic transmission factors through 13 excised skulls of male Sprague-Dawley rats weighing between 90 and 520 g, at different positions on each skull and at 1, 1.25, 1.5, 1.75 and 2 MHz. Our results revealed that insertion loss through rat skull increases linearly with both body mass and frequency and strongly depends on the position, decreasing from the front to the back and from the midline to the lateral sides. Skull thickness also scales linearly with body mass. Reflection explains the main part of the insertion loss compared with attenuation and aberration. These data are helpful in predicting the acoustic pressure at the focus in the brain. (E-mail: benoit.larrat@cea.fr)

Key Words: **Acoustic transmission, Insertion loss, Eat skull, Focused ultrasound.**

INTRODUCTION

In recent years, transcranial focused ultrasound (FUS) in the brain has emerged as a very promising therapeutic tool to replace or complement state-of-the-art therapies. For example, spectacular improvements have been observed in the tremor conditions of drug-resistant patients by thermally ablating tiny areas deep in the brain in a remote way (Elias et al. 2016). For all *in vivo* transcranial applications, precise knowledge of the peak negative pressure (PNP) at the focus is key to ensuring both the efficiency and safety of the procedures. Indeed, the acoustic pressure is directly related to the energy deposition in the tissues. This energy deposition must be sufficient to trigger the desired biological effects while avoiding undesired effects at the focus or out-of-focus lesions.

As an example, in high-intensity focused ultrasound for thermal ablation, the temperature rise has to be high enough to ablate cancerous cells (Dervishi et al. 2013; Pauly et al. 2006) or regions of the thalamus for essential tremor (Elias et al. 2016), yet the energy deposition must be controlled to prevent burning of the surrounding tissue (Shea et al. 2017).

Another promising application of FUS in the brain is the temporary blood–brain barrier opening (Hynynen et al. 2001). Combined with microbubbles injected in the blood flow, low-intensity FUS can permeate the vessel walls and allow drugs to enter the brain (Aryal et al. 2014; Marty et al. 2012). In this case, the PNP must be high enough to ensure significant oscillations of the circulating microbubbles to exert mechanical stress on vascular endothelium (McDannold et al. 2008) while staying low enough to strictly avoid implosion of microbubbles and permanent damage to the endothelial cells of the blood vessels (McDannold et al. 2012). Transcranial neurostimulation also strongly depends on the use of adequate intensity and control of the pressure distribution behind the skull (Deffieux et al. 2013). Reversibly, new transcranial imaging modalities that are developed at the pre-clinical stage thus far, such as functional ultrasound imaging (Tiran et al. 2017), photoacoustic imaging (Lavaud et al. 2017) and passive cavitation detection (Arvanitis et al. 2016), benefit from a good knowledge of skull attenuation and heterogeneity, thereby allowing for a gauge of the sensitivity required for the design of acoustic detectors.

Address correspondence to: Benoit Larrat, Centre CEA Saclay-Neurospin Bat 145, University Paris Saclay, 91191 Gif-sur Yvette, France. E-mail: benoit.larrat@cea.fr

To estimate PNP *in situ*, the first step is to calibrate the ultrasound transducer in a water tank. A second and influential step is correction for ultrasound insertion loss through the skull. The insertion loss results from the addition of several effects contributing to a decrease in the PNP at focus: aberration, reflection, absorption and scattering. The global skull insertion loss strongly depends on the animal species (Porto et al. 2013) because skull thickness, skull shape and bone structure are unique to each species. Even among a given species, skull insertion loss varies between individuals, especially in large animals (Asahara 2013) and from one skull location to another.

Most new FUS developments are first performed in rodents. Because it is larger compared with the mouse, the rat is a widely used animal model (Magnin et al. 2015; Mead et al. 2017; Yuan et al. 2016). Unfortunately, only one previous study has reported on the attenuation of rat skulls (O'Reilly et al. 2012). That study used skulls from Wistar rats weighing from 250 to 550 g. The authors reported a linear dependency of acoustic insertion loss with body mass at submegahertz frequencies, but no dependency at higher frequencies.

In the study described here, we investigated a larger range of body mass (90−520 g) and a different rat strain, Sprague-Dawley. We focus our measurements in the 1- to 2-MHz range.

METHODS

Acoustic setup

The transducer used for this study was a mono-element concave MR-compatible (diameter = 25 mm, focal depth = 20 mm; Imasonic, Voray-sur-l'Ognon, France) transducer with a central frequency of 1.5 MHz. The transducer was previously calibrated in a de-gassed water tank, and the focal spot was mapped at different frequencies ranging from 1 to 2 MHz. The transducer was mounted on a fixed holder in the tank filled with de-ionized water. A calibrated hydrophone (HGL-0200, preamplifier AH-2020, Onda, Sunnyvale, CA, USA) was used to measure acoustic pressures. Its active surface at the tip is a 200-μm-diameter disk. It was mounted on a micrometric three-axis positioning stage and placed in front of the transducer. The transducer was driven by a portable generator and amplifier (Image Guided Therapy, Pessac, France).

For all measurements, the pulses were 10 periods long with a 0.1-s pause between pulses. Two periods at the beginning and at the end of each pulse were excluded to ensure a purely monochromatic measurement. The electrical power was set to obtain an approximately 0.8-MPa PNP at focus in free water (at 1.5 MHz). The signal acquired by the hydrophone was directed to an oscilloscope (WaveRunner 44Xi, LeCroy, Chestnut Ridge, NY, USA), and the signal was an average of 50 measurements. The peak-to-peak voltage was measured on screen and converted into acoustic pressure thanks to the calibration data provided by the hydrophone manufacturer.

Skulls

Thirteen skulls were excised from Sprague-Dawley male rats ranging from 90 to 520 g in body mass. The skulls were obtained from previous studies approved by our local ethics committee (Project Authorization No. 12-058, Site Authorization No. B-91-272-01). After removal of as much tissue as possible, the skulls were boiled in a solution of water and sodium bicarbonate and then preserved in phosphate-buffered saline with azide. Skulls were never dry stored. The skulls, mounted on a micrometric three-axis positioning stage, were placed in the water tank. The water de-gassed for 15 min prior to any measurement. The de-gassing system was provided by Image Guided Therapy. The skulls were placed so that the focal spot of the ultrasound beam was approximately 5 mm under the skull, to mimic a realistic *in vivo* experiment with this transducer. The skulls were visually oriented with a normal incidence. The whole cone of the ultrasound beam intersected the skull for all measurements. The distance between the transducer center and skull surface was kept roughly constant for all measurements (16 ± 1 mm), which made the beam cross the skull over a circular surface 6 ± 1 mm in diameter.

Transmission measurements

For all acoustic measurements through skulls, the hydrophone was moved on the three axes to find the maximum pressure. It is to be noted that this location was never found to be farther than 0.1 mm from its location without the skull. The transmission factor was then defined as the ratio

$$\tau = P_{\text{skull}}/P_{\text{free}} \quad (1)$$

where P_{skull} is the acoustic pressure at the focus through the skull, and P_{free} the acoustic pressure at focus in free water. The voltage in output of the hydrophone was proportional to the acoustic pressure, and the transmission factor was directly calculated by obtaining the ratio of the voltages.

In the first experiment, three transmission measurements were done on 10 skulls at three different positions along the interhemispheric line—front, middle and back—as illustrated in Figure 1. The front position corresponds to the striatum, often used in diffusion experiments after ultrasound induced blood−brain barrier opening (Magnin et al. 2015) or to implant tumors for ultrasound treatments (Sun et al. 2017). The middle

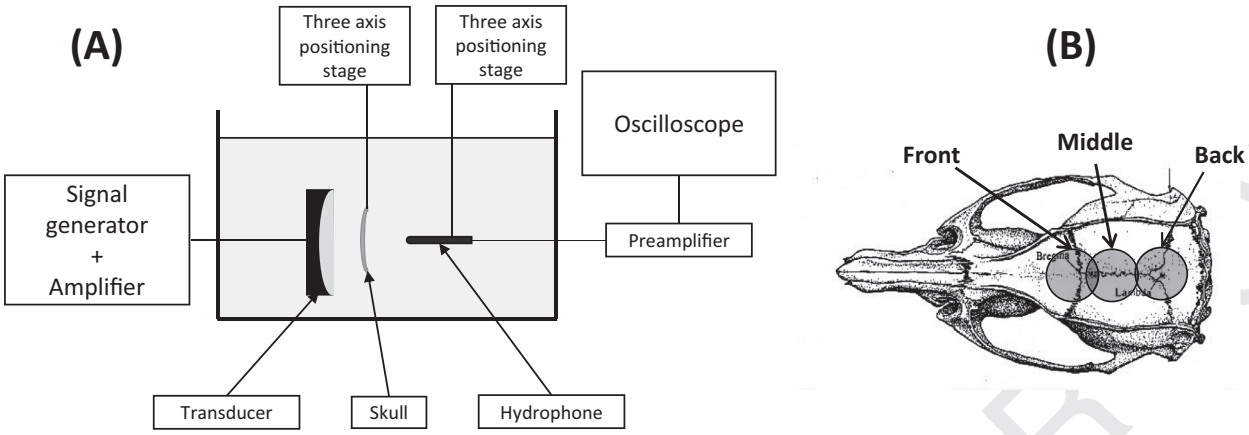

Fig. 1. (A) Setup for measurements of acoustic transmission in a water tank filled with de-ionized, de-gassed water. (B) Surfaces of the intersection of the ultrasound beam on the skull for the three different positions, for illustration purposes.

position corresponds to the hippocampus, a common target in studies on Alzheimer's disease models (Burgess et al. 2014). The back position corresponds to the cerebellum, an interesting region often used as a reference. Three skulls were missing the back part (behind lambda), lost during extraction of the skull. Five frequencies were studied (1, 1.25, 1.5, 1.75 and 2 MHz). After the transmission measurements, the skulls were carefully cut at the three positions (front, middle, and back) to measure their thicknesses with a caliper. Two measurements were done and averaged per position, one on each hemisphere. Unfortunately, one skull could not be measured in thickness, and two others could not be measured at the back position, resulting in thickness measurements for nine, nine and four skulls at the front, middle and back positions, respectively.

In a second experiment, the transmission factors of the left hemisphere of three additional skulls were mapped by translating the skulls millimeter by millimeter in a plane perpendicular to the axis of the transducer. These measurements were done at 1.5 MHz only. The scanning range was 7 mm in the left-to-right direction and 12 to 15 mm in the head-to-foot direction.

RESULTS

Transmission as a function of frequency and body mass

Figure 2 illustrates that the transmission factor decreases linearly with body mass of the rats, at each frequency and at each position (front, middle and back). The equations of the linear regressions and R^2 values are provided in Figure 2. Ninety-five percent confidence intervals for the parameters of the linear regression are given in Table 1. As illustrated in Figure 3, when averaging on position and body mass, the transmission factors decrease linearly ($R^2 = 0.99$) with frequency.

On the basis of this observation of the linear dependency of the transmission on body mass and frequency, a bilinear regression of the data was performed at each position, according to the equation

$$\tau = a + b \cdot \text{mass} + c \cdot \text{frequency} \quad (2)$$

Values and 95% confidence intervals of *a, b*, and *c* are given in Table 2.

The spreading of the focal spot was measured on a 280-g rat for the middle position. The width of the focal spot behind the skull was 1.55, 1.24 and 0.95 mm at 1, 1.5 and 2 MHz, compared with 1.46, 1.23 and 0.91 mm without the skull. The length of the focal spot behind the skull was 8.28, 5.73 and 4.95 mm at 1, 1.5 and 2 MHz, compared with 8.15, 5.85 and 4.53 mm without the skull.

Correlation with skull thickness

After cutting the skulls, measurements of their thickness obtained with a caliper are given in the plot in Figure 4A. It appears that the skull thickness, at each position, is proportional to the body mass. Skull thicknesses at the front and middle positions are very alike in both their absolute value and their dependence on body mass, unlike thickness at the back, which is higher and increases faster with increasing body mass. Figure 4B illustrates transmission factor as a function of skull thickness for 1.5 MHz and its linear regression for the front and middle positions. The linear regression includes only those two positions because measurements at the back seem to follow a different law. The linear regressions for the five frequencies are given in Table 3. On the linear regressions, it can be seen that the transmission factor tends to be 1 when the skull thickness tends to be 0, as expected. The slopes of the linear regressions become steeper with increasing frequency.

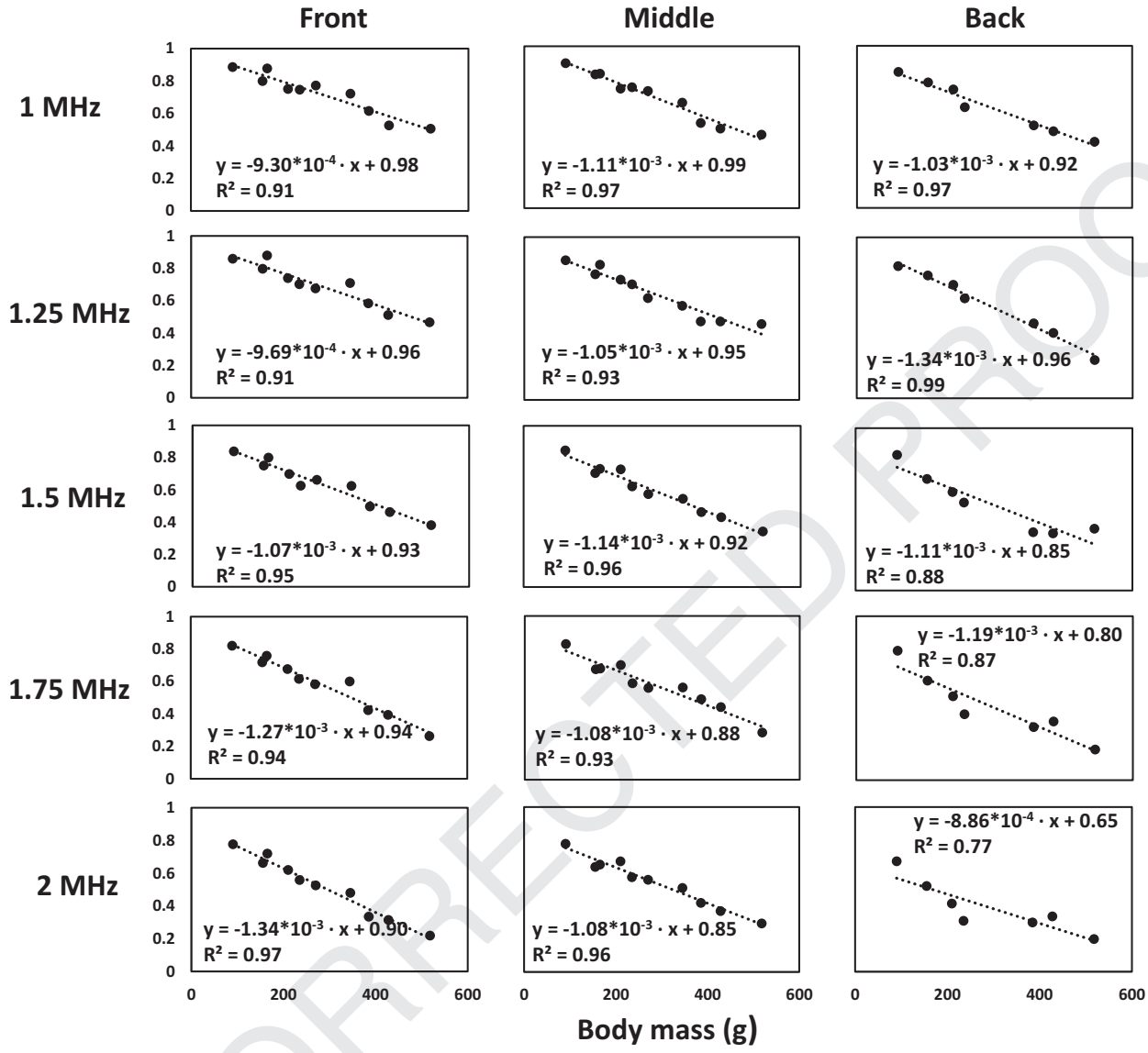

Fig. 2. Transmission factor as a function of body mass (g) for the five frequencies (1, 1.25, 1.5, 1.75 and 2 MHz) and three positions (front, middle, back). A linear regression and its equation are given for each graph.

Table 1. 95% Confidence intervals for parameters of the linear regression of τ as a function of animal body mass

		Position		
Frequency (MHz)	$\tau = a + b \cdot$ mass (g)	Front	Middle	Back
1	a	[0.907; 1.05]	[0.947; 1.05]	[0.853; 0.988]
	b (× 1000)	[−1.17; −0.689]	[−1.27, −0.940]	[−1.24; −0.824]
1.25	a	[0.882; 1.00]	[0.879; 1.01]	[0.905; 1.02]
	b (× 1000)	[−1.12; −0.722]	[−1.27; −0.828]	[−1.51; −1.16]
1.5	a	[0.873; 0.997]	[0.867; 0.975]	[0.833; 0.988]
	b (× 1000)	[−1.27; −0.871]	[−1.31, −0.9655]	[−1.61; −1.14]
1.75	a	[0.870; 1.01]	[0.811; 0.957]	[0.632; 0.965]
	b (× 1000)	[−1.49; −1.04]	[−1.32; −0.845]	[−1.71; −0.679]
2	a	[0.844; 0.953]	[0.797; 0.903]	[0.468, 0.828]
	b (× 1000)	[−1.52; −1.17]	[−1.26; −0.911]	[−1.44; −0.328]

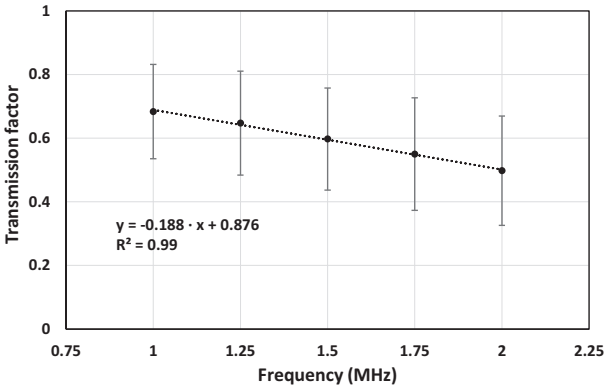

Fig. 3. Transmission factor as a function of frequency (MHz). For each frequency, an averaged (means ± standard deviations are shown) transmission factor on all skulls and all three positions is calculated. The parameters of the linear regression $\tau = a \cdot \text{frequency} + b$ with 95% confidence intervals: $a = -0.188$ [−0.208; −0.167] and $b = 0.876$ [0.845; 0.908].

Spatial variation of the transmission factor

As illustrated in Figure 5, the transmission factor also strongly depends on the region of skull intersected. In accordance with the above data illustrated in Figure 2, the overall transmission factor is higher for the 180- and 240-g skulls than for the 320-g skull. When moving left to right from the central suture to the sides of the skull, the transmission factor decreases rapidly from 68%, 64% and 59% to 43%, 41% and 30% for the 180-, 240- and 320-g skulls, respectively. This lateral decrease is hypothesized to come mainly from the beam incidence angle, which becomes less orthogonal to the skull surface, increasing reflection and so insertion loss, rather than from skull thickness variations. The transmission factor also decreases continuously when moving toward the back of the skull, as in previous measurements done at three discrete positions. The transmission factor decreases from 68%, 64% and 59% to 48%, 49% and 38%, respectively, for the three measured skulls when moving toward the back of the skulls.

DISCUSSION

Our study indicates a strong dependency of the acoustic transmission of rat skulls on body mass, position and frequency in the frequency range 1 to 2 MHz. These data are particularly useful for therapeutic applications of transcranial ultrasound. Indeed, an accurate knowledge of PNP is critical for most of these applications. For instance, it was proved by several groups that efficient and safe blood−brain barrier opening could be obtained in rats using only a narrow range of *in situ* focal pressure, typically 0.3 to 0.5 MPa at 1.5 MHz (Kobus et al. 2015). Below this range, no opening is observed because circulating microbubbles do not cavitate strongly enough, whereas above this range, inertial cavitation can be detected, resulting in permanent damage.

The skull extraction procedure, especially the boiling process, is thought not to change the acoustic properties of the bones. Indeed, as reported in Bosch et al. (2011), boiling bones does not change their structure or composition. They reported a change only in smoothness for boiling times longer than 4 h (our skulls were boiled for only 1 h) and at a nanometric level.

One group measured transmission factors at 1.5 MHz in Sprague-Dawley rats weighing from 300 to 400 g and with the exact same *f*-number of 0.8 and depth of focusing through the skull as in Treat et al. (2007). They found an average acoustic transmission of 51% in targeted regions close to the hippocampus, which would correspond to our middle region. For this region, at 1.5 MHz, for body masses between 300 and 400 g, we measured an average transmission factor of 53%. Their measurements, performed with parameters closely matching ours, correspond extremely well with our linear regression of the transmission factor as a function of body mass.

These results depend on the surface of intersected skull and, therefore, on the beam geometry. This study was performed with a relatively small transducer at low *f*-number (0.8). A relatively small surface of intersection of the beam with the skull enabled us to see the spatial dependency of the transmission factor as the ultrasound beam crosses completely different parts of the skull for the three measured positions. In particular, the front and middle positions appeared much less attenuated than the back position, where the skull is much thicker. We can expect that a larger transducer (i.e., a larger ultrasound beam) would average this spatial dependency by intersecting a larger surface of skull.

Table 2. Bilinear analysis of transmission factor τ as a function of body mass and frequency

	Value and 95% confidence interval		
$\tau = a + b \cdot \text{mass (g)} + c \cdot \text{frequency (MHz)}$	Front	Middle	Back
a	1.238 ± 0.058	1.134 ± 0.046	1.195 ± 0.094
b (× 1000)	−1.107 ± 0.088	−1.092 ± 0.073	−1.166 ± 0.135
c	−0.1989 ± 0.0336	−0.1425 ± 0.0264	−0.2318 ± 0.0557
R^2	0.94	0.96	0.92

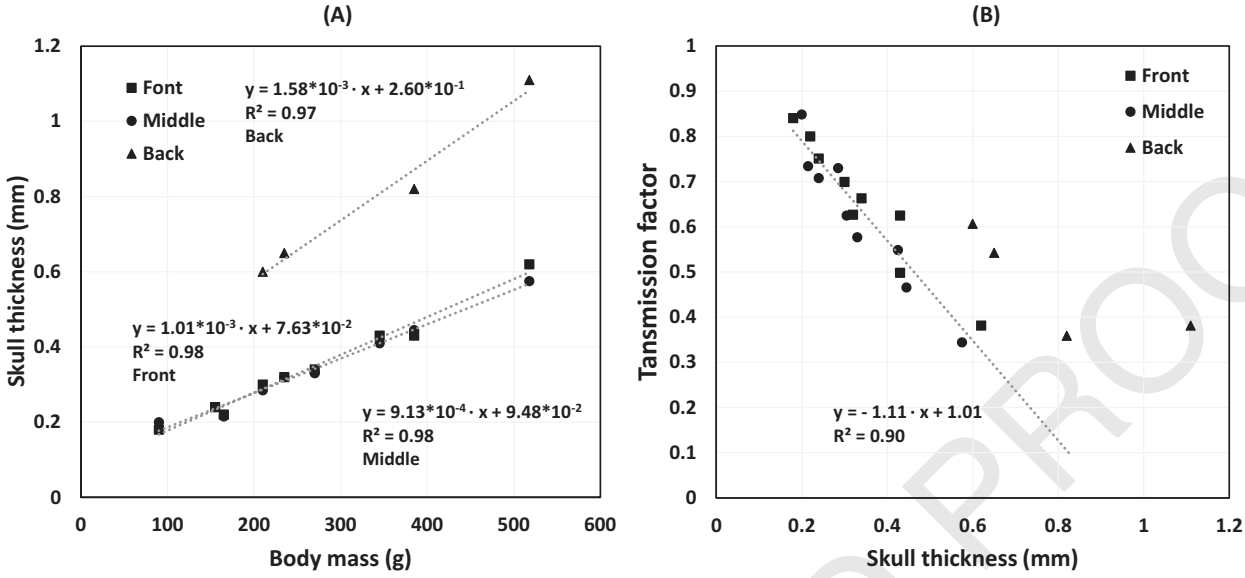

Fig. 4. (A) Skull thickness at three positions as a function of animal body mass. Linear regressions and their equations are given for each position. (B) Transmission factor as a function of skull thickness for all skulls and all positions, at 1.5 MHz. A Linear regressions for the front and middle positions and their equations are provided.

Globally, the transmission factor decreases linearly with body mass and is higher at the front and middle positions than at the back of the brain. Indeed, skull thickness is much larger at the back. Interestingly, this increased thickness does not fully translate into increased attenuation because when looking at the plot of transmission factor as a function of thickness (Fig 4B), larger thicknesses at the back often give transmission factors equal to those obtained for thinner skulls at more frontal positions. This could be explained by the increased curvature at the back resulting in an incidence angle systematically normal to the skull for the whole transducer aperture and/or by a more porous structure of the bone at the back, decreasing attenuation and impedance mismatch.

In healthy animals, our range of body mass roughly corresponds to an age of 30 to 70 days for rats weighing between 90 g and 400 g and an age older than 4 months for the 520-g rats (Lillie et al. 1996). Thus, most rats were young adults. Age can affect bone structure and density and hence the acoustic impedance (Jast and Jasiuk 2013). However, this change in bone density did not seem to affect our results, as results for the 520-g rat were consistent with those for the younger rats.

Table 3. Parameters of the linear regression of τ as a function of skull thickness

	$\tau = a + b \cdot$ skull thickness (mm)		
Frequency (MHz)	a	b	R^2
1	−0.9784 ± 0.1746	1.058 ± 0.062	0.89
1.25	−0.9964 ± 0.2019	1.030 ± 0.072	0.87
1.5	−1.106 ± 0.191	1.012 ± 0.069	0.90
1.75	−1.192 ± 0.208	1.006 ± 0.075	0.90
2	−1.215 ± 0.179	0.9673 ± 0.0643	0.93

Figure 6 illustrates the optical transparency of an adult rat skull of about 500 g. Diffuse white light is transmitted through the skull and exhibits a qualitatively higher bone density and/or thickness at the back versus the front of the head.

Skull aberration could explain part of the insertion loss as it can spread the focal spot behind the skull. No direct measurement of the phase was done. Nevertheless, few measurements suggest that aberration was not a main component of the insertion loss. As already mentioned, the location of the maximum pressure behind the skull was never found to be farther than 0.1 mm from its location without the skull, and the spreading of the focal spot behind the skull was small. Thus, both the displacement and the spreading of the focal spot remained very limited. This agrees with the finding reported by O'Reilly et al. (2012). Indeed, they measured a severe phase change at only 2.53 MHz and not up to 2 MHz and for "thicker animal skulls." In their study, skull thicknesses ranged from 0.5 to 1 mm, whereas the thicknesses in our study were always less than 0.5 mm for the front and middle positions. However, this may explain why at 2 MHz and for the back position, where the wavelength is closer to skull thickness (the shorter wavelength used was 1.45 mm at 2 MHz, with a speed of sound of 2900 m/s in bones, as reported by Fry and Barger in 1978, and the thicker skull portion is 1.06 mm at the back position), the correlation between body mass and transmission factor is the poorest ($R^2 = 0.77$). In this

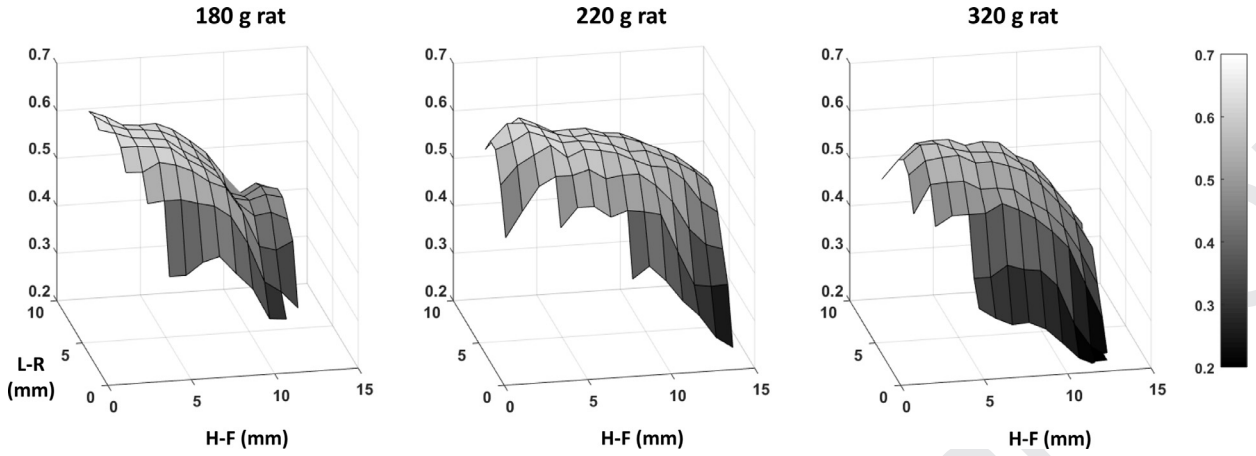

Fig. 5. Transmission factor at 1.5 MHz as a function of position of the skull between the transducer and hydrophone. From the left to the right of each surface, the skulls are mapped in the head-to-foot direction, starting from the front position. From the top to the bottom of each surface, skulls are mapped in the left-to-right direction, starting from the middle suture.

case, aberration might be non-negligible and deteriorate the relationship between body mass and transmission factor.

Attenuation and reflections are the two main components of the insertion loss, with the aberrations being negligible. Given the reported attenuation values for bone, $\alpha = 6.9$ dB/cm/MHz (Culjat et al. 2010), we calculated skull insertion losses caused by attenuation for all our specimens at 1.5 MHz with the equation (Cobbold 2007)

$$P = P_0 e^{-\alpha x} \quad (3)$$

where P_0 is the acoustic pressure before the skull, P is the acoustic pressure after the skull and x is the thickness of the skull. For all skull thicknesses, the part of insertion loss that can be attributed to attenuation remains low, between 10% and 20%. The remaining part of the measured insertion loss (80% to 90%) is expected to come from the impedance mismatch at the water−skull interface.

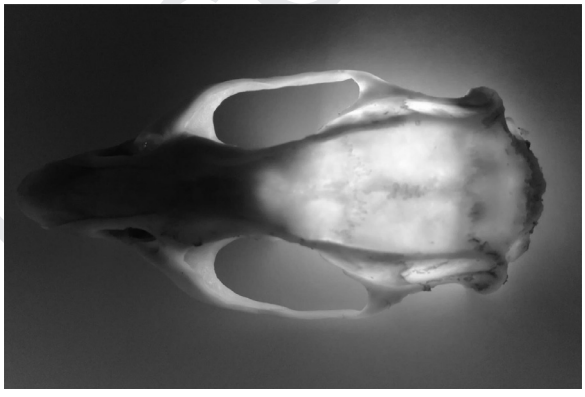

Fig. 6. Transparency image of a rat skull illuminated by white light, evidencing the increased thickness at the back compared with the front.

O'Reilly et al. (2012) concluded for the absence of dependency on the body mass in our frequency range, whereas our results exhibit a strong dependency on these parameters. Indeed, it is likely that the skull reaches the final developmental state for a given body mass. This plateau of thickness and calcification state should depend on the rat strain because it is well known that different strains have different growth (Baskin et al. [1979] for Fischer, Lillie et al. [1996] for Sprague-Dawley, and Goodrick [1980] for Wistar) and calcification speeds. Although this observation is only qualitative because of the small number of specimens tested, it could actually explain O'Reilly et al.'s conclusions because they used only Wistar rats larger than 250 g. In our case, our results summarized in Table 2 remain valid for Sprague-Dawley rats weighing up to 500 g and for frequencies ranging from 1 to 2 MHz. Indeed, aberrations are expected to increase significantly above 2 MHz, which would alter the linear behavior at higher frequencies. At lower frequencies, reflections on the bottom part of the skull that was removed in our measurements are expected to induce standing waves and change the pressure distribution in the brain.

Regarding the beam incidence angle, the lateral spatial dependency of the transmission factor found when mapping a whole hemisphere of three skulls most likely results from reflections caused by the curvature of the skull rather than attenuation. Indeed, the skull is moved perpendicularly to the axis of the transducer, meaning that moving sideways causes the ultrasound to go through a wider and less normal bone section, thus increasing the reflection and decreasing the transmission factor. Estimated on 3-D magnetic resonance images of

rats with the same body mass, the maximum incidence angle between the plane normal to the ultrasound beam and the plane tangent to the skull is about 65°.

Such a data set will help calibrate the ultrasound beam *in vivo* at first order. However, several experimental variables that cannot always be precisely controlled *in vivo* could strongly affect this calibration, mainly acoustic coupling (bubble trapping), beam incidence angle at the skull surface and multiple reflections in the whole skull cavity. To confirm the true *in situ* acoustic pressure and, if needed, to adjust it further, one should also rely on indirect *in situ* measurements during the in vivo intervention. For instance, under magnetic resonance imaging guidance, acoustic radiation force imaging (Larrat et al. 2010a, 2010b) can be used as an independent measurement of the acoustic intensity right before the intervention. Then, during FUS therapy, other indirect monitoring techniques, such as magnetic resonance thermometry (Larrat et al. 2010) and passive cavitation detection (Arvanitis et al. 2016), can be used in a feedback loop to adjust acoustic power on the fly.

Q2 **UNCITED REFERENCES:**

Keenan et al., 1997

Acknowledgments—The authors thank the CEA "Technologies for Health" transverse program, which funded this work.

REFERENCES

Arvanitis C, Crake C, McDannold N, Clement G. Passive acoustic mapping with the angular spectrum method. IEEE Trans Med Imaging 2016;36:983–993.

Aryal M, Arvanitis C, Alexander P, McDannold N. Ultrasound-mediated blood−brain barrier disruption for targeted drug delivery in the central nervous system. Adv Drug Deliver Rev 2014;72:94–109.

Asahara M. Shape variation in the skull and lower carnassial in a wild population of raccoon dog (*Nyctereutes procyonoides*). Zool Sci 2013;30:205–210.

Baskin S, Roberts J, Kendrick Z. Effect of age on body weight, heart rate and blood pressure in pair-caged, male, Fisher 344 rats. Age 1979;2:47–50.

Bosch P, Aleman I, Moreno-Castilla C, Botella M. Boiled versus unboiled: A study on Neolithic and contemporary human bones. J Archaeol Sci 2011;38:2561–2570.

Burgess A, Dubey S, Yeung S, Hough O, Eterman N, Aubert I, Hynynen K. Focused ultrasound targeted to the hippocampus opens the blood−brain barrier and improves pathologic abnormalities and behavior. Radiology 2014;273:736–745.

Cobbold RSC. Foundations of biomedical ultrasound. Oxford: University Press; 2007.

Culjat M, Goldenberg D, Tewari P, Singh R. A review of tissue substitutes for ultrasound imaging. Ultrasound in Med Biol 2010;36:861–873.

Deffieux T, Younan Y, Wattiez N, Tanter M, Pouget P, Aubry JF. Low-intensity focused ultrasound modulates monkey visuomotor behavior. Curr Biol 2013;23:2430–2433.

Dervishi E, Larrat B, Pernot M, Adam C, MarieY FinkM, Delattre JY, Boch AL, Tanter M, Aubry JF. Transcranial high intensity focused ultrasound therapy guided by 7 Tesla MRI in a rat brain tumour model: A feasibility study. Int J Hyperthermia 2013;29:598–608.

Elias J, Lipsman N, Ondo W, Ghanouni P, Kim Y, Lee W, Schwartz M, Hynynen K, Lozano A, Shah B, Huss D, Dallapiazza R, Gwinn R, Witt J, Ro S, Eisenberg H, Fishman P, Gandhi D, Halpern C, Chuang R, Pauly K, Tierney T, Hayes M, Cosgrove R, Yamaguchi T, Abe K, Taira T, Chang J. A randomized trial of focused ultrasound thalamotomy for essential tremor. N Engl J Med 2016;375:730–739.

Fry F, Barger J. Acoustical properties of the human skull. J Acoust Soc Am 1978;63:1576–1590.

Goodrick C. Effects of long-term voluntary wheel exercise on male and female Wistar rats. Gerontology 1980;26:22–33.

Hynynen K, McDannold N, Vykhodtseva N, Jolesz F. Noninvasive mr imaging-guided focal opening of the blood−brain barrier in rabbits. Radiology 2001;220:640–646.

Jast J, Jasiuk I. Age-related changes in the 3D hierarchical structure of rat tibia cortical bone characterized by high-resolution micro-CT. J Appl Physiol 2013;114:923–933.

Keenan M, Hegsted M, Jones K, Delany J, Kime J, Melancon L, Tulley R, Hong K. Comparison of bone density measurement techniques: DXA and Archimede's principle. J Bone Miner Res 1997;12:1903–1907. Q3

Kobus T, Vykhodtseva N, Pilatou M, Zhang Y, McDannold N. Safety validation of repeated blood−brain barrier disruption using focused ultrasound. Ultrasound Med Biol 2015;42:481–492.

Larrat B, Pernot M, Aubry JF, Dervishi E, Sinkus R, Seilhean D, Marie Y, Boch AL, Fink M, Tanter M. MR-guided transcranial brain HIFU in small animal models. Phys Med Biol 2010;55:365–388.

Larrat B, Pernot M, Montaldo G, Fink M, Tanter M. MR-guided adaptive focusing of ultrasound. IEEE Trans Ultrason Ferroelectr Freq Control 2010;57:1734–1747.

Lavaud J, Henry M, Coll JL, Josserand V. Exploration of melanoma metastases in mice brains using endogenous contrast photoacoustic imaging. Int J Pharm 2017;532:704–709.

Lillie L, Temple N, Florence Z. reference values for young normal Sprague-Dawley rats: Weight gain, hematology and clinical chemistry. Hum Exp Toxicol 1996;15:612–616.

Magnin R, Rabusseau F, Salabartan F, Mériaux S, Aubry JF, Le Bihan D DumontE, Larrat B. Magnetic resonance-guided motorized transcranial ultrasound system for blood−brain barrier permeabilization along arbitrary trajectories in rodents. J Ther Ultrasound 2015;3(1):22.

Marty B, Larrat B, Van Landeghem M RobicC, Robert P, Port M, Denis Le Bihan D, Pernot M, Tanter M, Lethimonnier F, Sebastien Meriaux S. Dynamic study of blood−brain barrier closure after its disruption using ultrasound: A quantitative analysis. J Cerebr Blood Flow Metab 2012;32:1948–1958.

McDannold N, Vykhodtseva N, Hynynen K. Blood−brain barrier disruption induced by focused ultrasound and circulating preformed microbubbles appears to be characterized by the mechanical index. Ultrasound Med Biol 2008;34:834–840.

McDannold N, Arvanitis C, Vykhodtseva N, Livingstone M. Temporary disruption of the blood−brain barrier by use of ultrasound and microbubbles: safety and efficacy evaluation in rhesus macaques. Cancer Res 2012;72:3652–3663.

Mead B, Kim N Miller W, Hodges D Mastorakos P, Klibanov A, Mandell J, Hirsh J, Suk J S, Hanes J, Price R. Novel focused ultrasound gene therapy approach noninvasively restores dopaminergic neuron function in a rat Parkinson's disease model. Nano Lett 2017;17:3533–3542.

O'Reilly M, Muller A, Hynynen K. Ultrasound insertion loss of rat parietal bone appears to be proportional to animal mass at submegahertz frequencies. Ultrasound Med Biol 2012;29:997–1003.

Pauly K, Diederich C, Rieke V, Bouley D, Chen J, Nau W, Ross B, Kinsey A, Sommer G. Magnetic resonance-guided high-intensity ultrasound ablation of the prostate. Top Magn Reson Imaging 2006;17:195–207.

Porto A, Shirai L, Bandoni de Oliveira F, Marroig G. Size variation, growth strategies, and the evolution of modularity in the mammalian skull. Evolution 2013;67:3305–3322.

Shea J, de Bever J, Kholmovski E, Beal H, Hadley R, Minalga E, Salama M, Marrouche N, Payne A. Effect of applied energy in renal

sympathetic denervation with magnetic resonance guided focused ultrasound in a porcine model. J Ther Ultrasound 2017;5:16.

Sun T, Zhang Y, Power C, Alexander P, Sutton J, Aryal M, Vykhodtseva N, Miller E, McDannold N. Closed-loop control of targeted ultrasound drug delivery across the blood−brain/tumor barriers in a rat glioma model. Proc Natl Acad Sci USA 2017;114:E10281–E10290.

Tiran E, Ferrier J, Deffieux T, Gennisson JL, Pezet S, Lenkei Z, Tanter M. Transcranial functional ultrasound imaging in freely moving awake mice and anesthetized young rats without contrast agent. Ultrasound Med Biol 2017;43:1679–1689.

Treat L, McDannold N, Vykhodtseva N, Zhang Y, Tam K, Hynynen K. Targeted delivery of doxorubicin to the rat brain at therapeutic levels using MRI-guided focused ultrasound. Int J Cancer 2007;121:901–907.

Yuan Y, Yan J, Ma Z, Li X. Noninvasive focused ultrasound stimulation can modulate phase−amplitude coupling between neuronal oscillations in the rat hippocampus. Front Neurosci 2016;10 (July):1–7.